Journal of The Electrochemical Society, **166** (6) A1103-A1106 (2019)
0013-4651/2019/166(6)/A1103/4/$38.00 © The Electrochemical Society

Electrochemical Performance of 1-Ethyl-3-Methylimidazolium Bis(Trifluoromethylsulfonyl)Imide Ionic Liquid as Electrolyte for Primary Mg-Air Batteries

Jingli Zhang,[1] Jingling Ma,[1,z] Guangxin Wang,[1,z] Yaqiong Li,[1] and Alex A. Volinsky[2]

[1]*Research Center for High Purity Materials, Henan University of Science and Technology, Luoyang 471023, People's Republic of China*
[2]*Department of Mechanical Engineering, University of South Florida, Tampa, Florida 33620, USA*

Ionic liquids are promising electrolytes for the primary Mg-air batteries. Three electrolytes, including pure 1-ethyl-3-methylimidazolium bis(trifluoromethylsulfonyl)imide ionic liquid, 50 mol.% butyl acetate and 50 mol.% water were studied. Attenuated total reflectance Fourier transform infrared spectroscopy, scanning electron microscopy and electrochemical impedance spectroscopy were used to examine discharge performance and the effects of butyl acetate and water additions. Galvanostatic measurements indicate that butyl acetate is an excellent additive, which can significantly improve the battery performance by reducing electrolyte impedance by increasing conductivity. However, while water also improved electrolyte discharge performance, it was consumed by the hydrogen evolution reaction over the 72 h discharge.
 [DOI: 10.1149/2.0821906jes]

Manuscript submitted January 22, 2019; revised manuscript received March 12, 2019. Published April 3, 2019.

Magnesium is a light, active metal with the standard potential of 2.37 V (vs. SHE) and potential capacity of −2,204 mA·h/g, as excellent as lithium and aluminum.[1–4] Therefore, it can be used as an electrode material in batteries.[5] In recent years Mg-air batteries have received increasing attention due to the high energy density of up to 6,450 W·h/kg and stable performance.[6,7] Ionic liquids (IL) have been used in metal-air batteries due to their negligible vapor pressure, high thermal and electrochemical stability and non-flammability.[8,9]

Khoo et al.[10–13] have used the Grignard reagent ionic liquids in Mg-air batteries. Their studies showed that the Grignard reagent stabilized the interface between the Mg anode and the electrolyte and reduced magnesium self-corrosion. The addition of water improved the electrolyte conductivity and changed the anode surface microstructure. Thus, the discharge performance of the Mg-air battery was optimized. Kuboki et al.[14] reported the improved performance of the lithium-air batteries with a hydrophobic ionic liquid consisting of 1-alkyl-3-methyl imidazolium cations and perfluoroalkylsulfonyl imide anions. Also, 1-ethyl-3-methylimidazolium bis(trifluoromethylsulfonyl)imide demonstrated excellent electrolyte performance.[14]

Additionally, 1-butyl-1-methylpiperidinium bis(trifluoromethylsulfonyl)imide ($PP_{14}TFSI$) ionic liquid was studied in dual-ion batteries,[15] Li-S cells[16] and in rechargeable batteries.[17] According to previous studies, water is a commonly used additive in ionic liquids. The possible roles of water have been identified. Water enhanced ion transport properties of IL by providing active protons to the cathodic oxygen reduction reaction. It also helped Mg^{2+} ions to form an amorphous interface layer, which supports Mg dissolution.[10,12,13,18] This paper studied the electrochemical behavior of the primary Mg-air battery using the $PP_{14}TFSI$ as the electrolyte and further explored the effects of H_2O and organic solvent butyl acetate (BA) additives. Previous studies found that H_2O enhances the IL conductivity due to its high dielectric constant,[19,20] and butyl acetate is a widely used organic solvent to improve the mass transfer performance of the electrolyte.[21] The aim of this research is to analyze the feasibility of the additives to improve the performance of the $PP_{14}TFSI$-based electrolytes in primary Mg-air batteries.

Experimental

Pure magnesium (99.95%) has been used as the anode. The air electrode was made up of a waterproof layer, catalytic layer, and current collector. The waterproof layer was made of 40 wt% acetylene black as a conductive material and 60 wt% poly(tetrafluoroethylene) (PTFE) as a binding material. The catalytic layer was made of 37.5 wt% MnO_2 and 25 wt% activated carbon as the catalyst and 37.5 wt% PTFE as a binding material. $PP_{14}TFSI$ was obtained from the Shanghai Cheng Jie Chemical Co. Ltd (Shanghai, China).

The electrochemical tests were performed using the CHI660C electrochemical workstation (CHI, USA). The open circuit potential (OCP) of working electrodes was measured using the 1 cm^2 exposed area. The electrochemical impedance spectroscopy (EIS) measurements were carried out at the OCP with a 5 mV sinusoidal modulation. The measurement frequency range was 10^{-2}-10^5 Hz, starting with the higher frequency.

Galvanostatic discharge experiments were conducted using the CT2001A Landt discharge test system (Wuhan Lan Sheng Electronic Technology Co. Ltd, Wuhan, China). The sample surface after discharge was examined using scanning electron microscopy (SEM, JSM-5610LV). The electrolyte chemical composition was studied by the attenuated total reflectance Fourier transform infrared spectroscopy (ATR-FTIR). Additionally, conductivity and viscosity were investigated by the FE38 standard conductivity gauge (Mettler Toledo Instruments Co. Ltd, Switzerland) and DV-97+Pro viscosity meter (Shanghai Nirun Technology Company, China), respectively at 25°C, to verify the electrochemical results and examine the effects of BA and H_2O.

Results and Discussion

The galvanostatic discharge curves and the ATR-FTIR spectra of the electrolytes are shown in Fig. 1. The discharge current density was 0.1 mA/cm^2 in each case. As seen in Fig. 1a, the operating voltage rapidly decreased in the early discharge stage, caused by the internal resistance of the battery, and then reached an approximately constant value for the consequent 72 h. Compared with the IL mixture (H_2O and BA added separately), the discharge performance of pure $PP_{14}TFSI$ exhibits instabilities, accompanied by lower voltage and more voltage fluctuations. Based on the discharge curves, H_2O and BA additions resulted in higher and more stable voltage.

In the initial 10 h of discharge, the voltage of $PP_{14}TFSI$ with 50 mol.% H_2O electrolyte gradually increased and declined thereafter. Normally, during the discharge process, the hydrogen evolution reaction occurs at the Mg anode:[22,23]

$$Mg + H_2O = Mg(OH)_2 + H_2 \quad [1]$$

The consumption of H_2O and the accumulation of $Mg(OH)_2$ may cause high electrical resistance of the electrolyte, resulting in deteriorated battery performance after 10 h of discharge. In this study, the action mechanisms of H_2O on $PP_{14}TFSI$ were analyzed in detail.

[z]E-mail: majingling@haust.edu.cn; wgx58@126.com

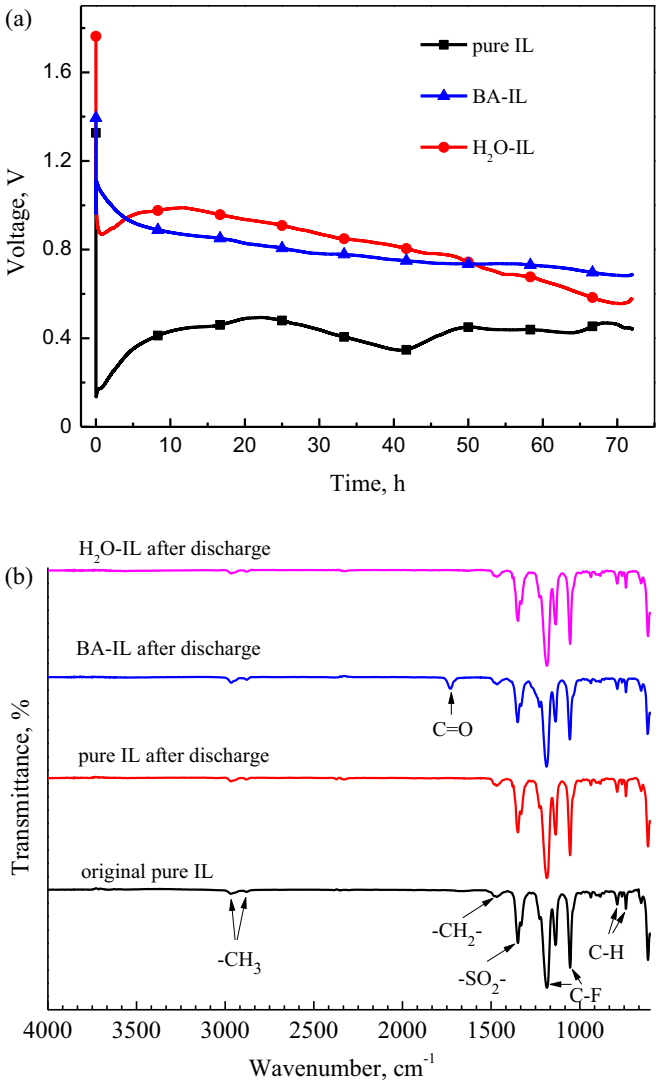

Figure 1. (a) Galvanostatic discharge curves and (b) ATR-FTIR spectra of electrolytes.

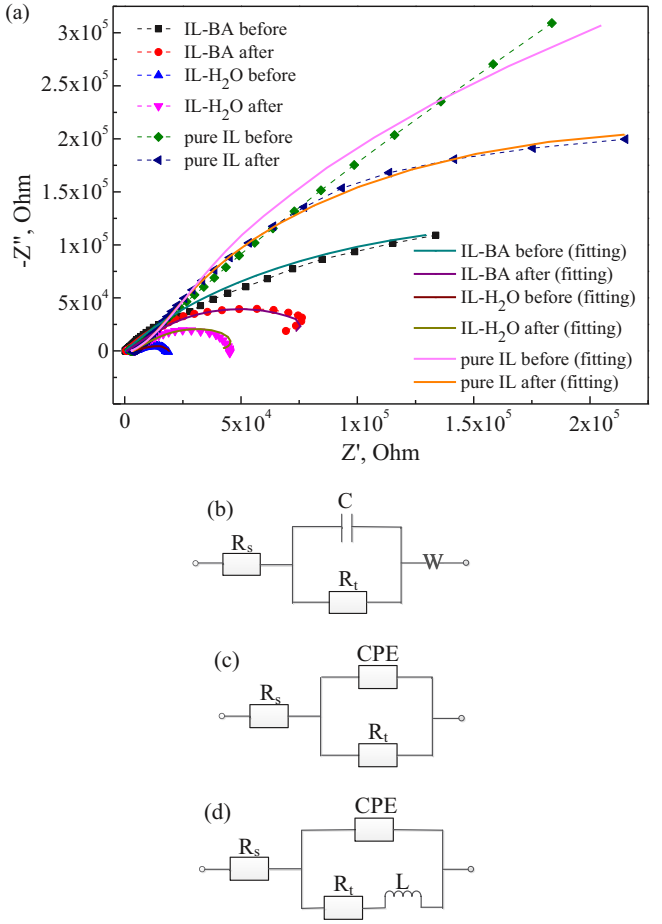

Figure 2. (a) EIS patterns of the three electrolytes before and after 72 h discharge; (b) Equivalent EIS circuits of pure IL before and after discharge; (c) Equivalent EIS circuits of BA-IL and H_2O-IL before discharge; (d) Equivalent EIS circuits of BA-IL and H_2O-IL after discharge.

The discharge curve of the $PP_{14}TFSI$ with 50 mol.% BA exhibits minimum fluctuations and BA has an outstanding performance over the 72 h galvanostatic discharge period, suggesting that BA is a stable additive for the $PP_{14}TFSI$.

As seen in Fig. 1b, the spectra from the original IL, IL after discharge and IL with added H_2O after discharge look quite similar. The chemical structure of $PP_{14}TFSI$ didn't change after 72 h discharge. This illustrates that $PP_{14}TFSI$ is a chemically stable electrolyte, which can withstand longer discharge. Lack of noticeable H_2O peak between 3550 cm^{-1} and 3230 cm^{-1} in the discharged H_2O-IL system implies that H_2O is involved in the hydrogen evolution reaction. The $PP_{14}TFSI$ BA mixture results are similar to the original pure $PP_{14}TFSI$. According to the BA-IL system spectra, the peak at 1728 cm^{-1} is assigned to the C=O bond of BA.[24] The ATR-FTIR results of the BS-IL system confirmed the effects of BA on the stability of $PP_{14}TFSI$.

The EIS plots of the three electrolytes before and after discharge are shown in Fig. 2a. BA and H_2O can effectively reduce the impedance and improve the mass transfer performance. The performance of H_2O is even more outstanding. Moreover, for the pure IL and 50 mol.% BA-IL systems, the resistance after discharge is obviously lower than before. This is perhaps caused by the collapse of the surface passivation layer on the Mg anode. However, the opposite result is observed in the 50 mol.% H_2O-IL. This is due to H_2O being consumed by the hydrogen evolution reaction during the discharge process. The capacitive loops in each electrolyte system are related to the interfacial electrochemical reactions and the interface charge transfer, although the capacitive loops of pure IL and BA-IL systems before discharge are incomplete. Noteworthy, sloped lines, which represent the diffusion process in the electrolyte, are obtained in the IL systems, indicating the difficulty of charge transfer in pure $PP_{14}TFSI$.[25]

To further investigate the impedance of the three systems, several equivalent circuits were constructed in Figs. 2b–2d. In Figs. 2b–2d, R_s represents the solution resistance, R_t and CPE or C are the charge transfer resistance and double layer capacitance of the Mg surface, and L is the inductance. W is the Warburg impedance, describing the diffusion process in pure IL electrolyte. The fitted values of the equivalent elements are listed in Table I. Low X^2 variance values reflect good fits of electrolytes impedance.

In Fig. 2b, the W element explains electric charge transfer difficulty in pure IL due to the enormous $PP_{14}TFSI$ ionic group size and high viscosity, causing large mechanical drag force. The lack of W element in Figs. 2c and 2d indicates that BA and H_2O make charge transfer more effective. The effects of BA and H_2O on viscosity are shown in Fig. 3a. Obviously, the viscosity decreased significantly with added BA, owing to its small molecular size and excellent miscibility with $PP_{14}TFSI$. The impact of H_2O on viscosity is relatively low but still plays its role on the charge transfer.

In Table I, the R_s parameter values suggest that BA can significantly reduce the solution resistance, but H_2O has no effect at all. Accordingly, the conductivity of the three electrolytes is shown in Fig. 3b, the

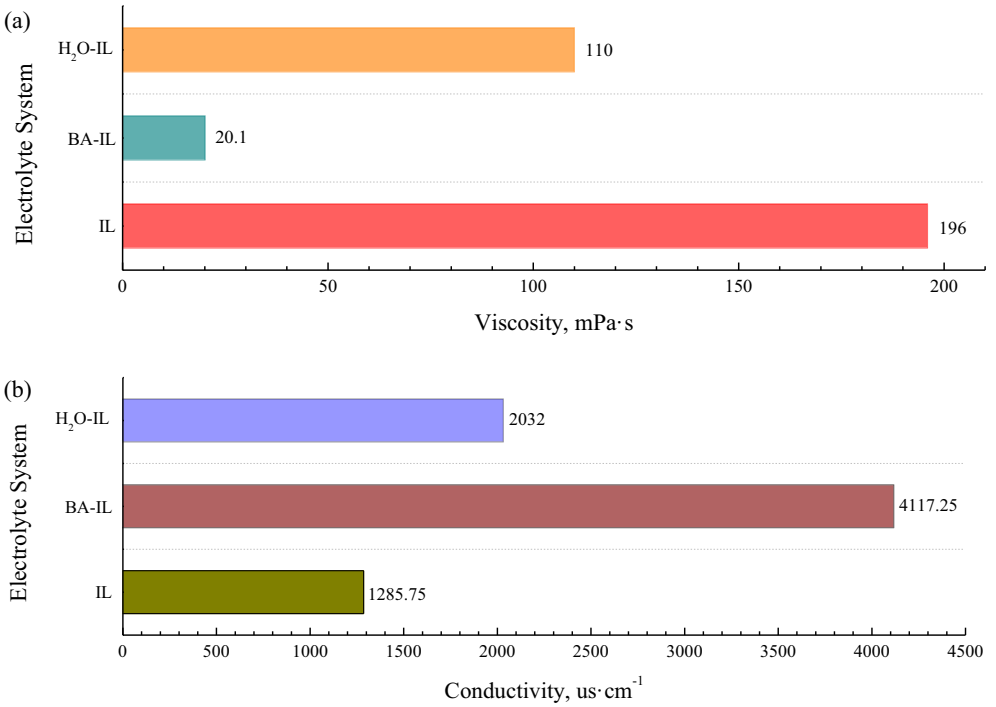

Figure 3. (a) Viscosity of the three electrolytes; (b) Conductivity of the three electrolyte.

results are in correspondence with R_s. Obviously, the consequences contradict to the coulomb force law:

$$F = \frac{Q1Q2}{4\pi\varepsilon_0\varepsilon_r r^2} \quad [2]$$

where F is the electrostatic force, Q1 and Q2 are point electric charges, ε_0 is vacuum permittivity, ε_r is relative permittivity of the medium, and r is the distance between the two charges. The electrostatic force inhibits the electrolytic dissociation, and with high force, most of the ionic species exist as ion pairs. Ion pairs contribute neither ionic strength nor ionic conductivity to the solution.[26] According to the coulomb force law, the electrostatic force of attraction between two ions with the opposite charge decreases with the increase of ε_r. The permittivity of BA and H_2O is 5.07 and 78.36 F/m respectively,[27] however, H_2O lost its proper role due to low solubility in IL. Thus it can be seen that both favorable miscibility and permittivity are necessary.

As for the interface processes, double layer capacitance C in pure IL in Fig. 2b is replaced by the CPE element in Figs. 2c and 2d, and the n parameter for the CPE is between 0.529 and 0.713 in Table I. This illustrates that H_2O and BA reduce the Mg anode interface stability.

Moreover, it is noteworthy that H_2O decreases the charge transfer resistance by one order of magnitude, which can be observed by comparing the R_t values in each system, revealing that H_2O plays an essential role in the interface process of charge transfer. For the H_2O-IL system, H_2O improved the chemical properties of the interface between Mg anode and an organic electrolyte solution and then promoted the electrochemical process of charge transfer by extracting it from the anode and transferring it to the electrolyte. The difficult degree of the charge transfer also can be reflected by the SEM images of the Mg anode surfaces before and after 72 h discharge in pure IL, 50 mol.% BA-IL and 50 mol.% H_2O-IL electrolytes, as shown in Fig. 4. In contrast, more pronounced discharge morphology could be seen on the Mg surface of H_2O-IL in Fig. 4f, which corroborated the positive effect of H_2O on the electrode/electrolyte interface, accompanying inevitable self-corrosion. The round-like bulges in Fig. 4f suggest that there was gas generated at the interface during the discharge process, which further proves hydrogen evolution on the Mg surface in the H_2O-IL system. Beyond that, the wide and deep cracks on the electrode locally of BA-IL in Fig. 4e and the morphology in Fig. 4f agree with the inductance results in Fig. 2d, representing intergranular corrosion of the Mg anode.

Table I. EIS elements values simulated using the corresponding equivalent circuits.

	Pure IL		BA-IL		H_2O-IL	
Electrolyte	Before	After	Before	After	Before	After
R_s ($\times 10^3$, $\Omega\cdot cm^2$)	2.699	3.102	0.27	0.809	3.552	3.389
CPE ($\times 10^{-5}$, $F\cdot cm^{-2}$)	-	-	3.048	3.515	4.087	4.473
n (0<n<1)	-	-	0.713	0.621	0.529	0.568
R_t ($\times 10^{5,}$ $\Omega\cdot cm$)	6.109	2.84	3.738	1.231	0.173	0.479
L ($\times 10^{5,}$ $H\cdot cm^2$)	-	-	-	5.332	-	2.049
C ($\times 10^{-5}$, $F\cdot cm^{-2}$)	4.576	5.315	-	-	-	-
W ($\times 10^{-5}$, $\Omega\cdot cm^2$)	3.652	4.537	-	-	-	-
Variance, X^2 ($\times 10^{-3}$)	2.091	7.224	6.351	5.848	7.843	5.842

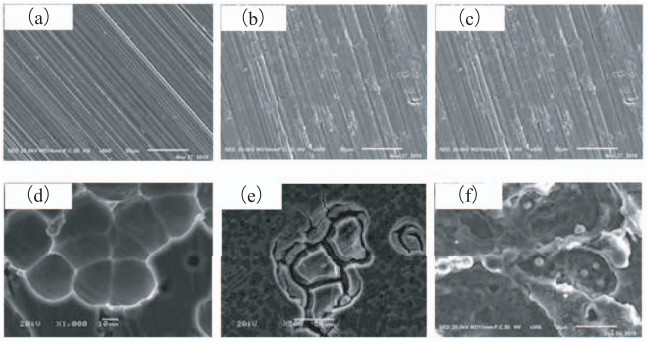

Figure 4. SEM micrographs of the Mg-anode in different electrolytes before and after 72 h discharge: (a) pure IL before, (b) BA-IL before, (c) H_2O-IL before, (d) pure IL after, (e) BA-IL after, (f) H_2O-IL after.

Further work is underway to research the mechanism and optimal dosage of additives. Obviously, the battery structure is also crucial and is currently under investigation.

Conclusions

Electrochemical performance of the $PP_{14}TFSI$ ionic liquid, BA-IL and H_2O-IL mixtures as an electrolyte for the Mg-air battery was investigated. The $PP_{14}TFSI$ ionic liquid can sustain 72 h discharge. BA increased the discharge voltage and made it more stable. Meanwhile, H_2O has a similar action, but the effect was degraded by the hydrogen evolution reaction. Based on the EIS, equivalent circuits, viscosity, conductivity and SEM results, both BA and H_2O have excellent performance in terms of improving electrolyte charge diffusion by decreasing electrolyte viscosity. Furthermore, BA reduces electrolyte impedance by increasing conductivity, and H_2O improves conductivity at the interface between the anode and the electrolyte.

Acknowledgments

This work was supported by the Chinese 02 Special Fund (2017ZX02408003), the Chinese 1000 Plan for the High-Level Foreign Experts (WQ20154100278), the Innovative Research Team Program of the Henan University of Science and Technology (2015XTD006), the National Science Foundation (IRES 1358088), and by the Natural Science Foundation of Henan Province (grant No. 182300410173).

ORCID

Jingli Zhang https://orcid.org/0000-0002-9130-5007
Guangxin Wang https://orcid.org/0000-0002-3137-1950

References

1. Z. Zhao-Karger, X. Zhao, and D. Wang, *Advanced Energy Materials*, **5**, 1401155 (2015) .
2. A. Kitada, Y. Kang, and Y. Uchimoto, *Journal of the Electrochemical Society*, **161**, 102 (2013).
3. Y. T. Law, J. Schnaidt, S. Brimaud, and R. J. Behm, *Journal of Power Sources*, **333**, 173 (2016).
4. T. Zhang, Z. Tao, and J. Chen, *Materials Horizons*, **1**, 196 (2014).
5. X. Zhao, Q. Li, Z. Zhao-Karger, P. Gao, K. Fink, X. Shen, and M. Fichtner, *ACS Applied Materials & Interfaces*, **6**, 10997 (2014).
6. M. Armand and J. M. Tarascon, *Nature*, **451**, 652 (2008).
7. F. Cheng and J. Chen, *Chemical Society Reviews*, **43**, 2172 (2012).
8. H. L. Zhang and W. J. Wang, *Modern Chemical Industry*, **22**, 13 (2002).
9. M. Armand, F. Endres, D. R. Macfarlane, H. Ohno, and B. Scrosati, *Nature Materials*, **8**, 621 (2009).
10. Y. J. Yan, Ph.D. Thesis, Deakin University, Victoria State, Australia. (2016).
11. Y. J. Yan, T. Khoo, C. Pozo-Gonzalo, A. F. Hollenkamp, P. C. Howlett, D. R. Macfarlane, and M. Forsyth, *Journal of the Electrochemical Society*, **161**, A974 (2014).
12. T. Khoo, A. Somers, A. A. J Torriero, and D. R. Macfarlane, *Electrochimica Acta*, **87**, 701 (2013).
13. T. Khoo, P. C. Howlett, M. Tsagouria, D. R. Macfarlane, and M. Forsyth, *Electrochimica Acta*, **58**, 583 (2011).
14. T. Kuboki, T. Okuyama, T. Ohsaki, and N. Takami, *Journal of Power Sources*, **146**, 766 (2005).
15. J. Fan, Z. Zhang, Y. Liu, A. Wang, L. Li, and W. Yuan, *Chemical Communications*, **53**, 6891 (2017).
16. B. Krik and M. S. Thesis, Charmers University of Technology, Gothenburg, Sweden. (2012).
17. J. J. Zhu, F. F. Wang, Y. S. Gao, J. Yang, N. Liyanna, and J. L. Wang, *Journal of Electrochemistry*, **20**, 128 (2014).
18. P. M. Bayley, J. Novak, T. Khoo, M. M. Britton, P. C. Howlett, and D. R. Macfarlane, *Australian Journal of Chemistry*, **65**, 1542 (2012).
19. I. Goodchild, L. Collier, S. L. Millar, I. Prokes, J. C. D. Lord, C. P. Butts, J. Bowers, J. R. P. Webster, and R. K. Heenan, *Journal of Colloid and Interface Science*, **307**, 455 (2007).
20. W. Li, Z. Zhang, B. Han, S. Hu, Y. Xie, and G. Yang, *Journal of Physical Chemistry B*, **111**, 6452 (2007).
21. B. Q. Jiang, Z. Q. Ye, X. X. Liu, X. Y. Yu, and W. L. Zhang, *Journal of Rare Earths*, **25**, 244 (2007).
22. G. G. Kumar and N. Munichandraiah, *Journal of Power Sources*, **91**, 157 (2000).
23. R. M. Dell, *Solid State Ionics*, **134**, 139 (2000).
24. P. Larkin, Infrared and Raman Spectroscopy: Principles and Spectral Interpretation. Elsevier, Netherlands, 63 (2011).
25. C. N. Cao and J. Q. Zhang, An Introduction to Electrochemical Impedance Spectroscopy, China Science Publishing & Media Ltd., Beijing, 86 (2011).
26. K. Izutsu, Electrochemistry in Nonaqueous Solutions, Wiley-VCH, Weinheim, 27 (2002).
27. W. M. Haynes, D. R. Lide, and T. J. Bruno, *CRC Handbook of Chemistry and Physics*, CRC Press, Florida, 6 (2014).